Numerical solutions of pulsating flow and heat transfer characteristics in a pipe

H. W. Cho and J. M. Hyun
Department of Mechanical Engineering, Korea Advanced Institute Science and Technology, Chong Ryang, Seoul, Korea

Numerical studies are made of flow and heat transfer characteristics of a pulsating flow in a pipe. Complete time-dependent laminar boundary-layer equations are solved numerically over broad ranges of the parameter spaces, i.e., the frequency parameter β and the amplitude of oscillation A. Recently developed numerical solution procedures for unsteady boundary-layer equations are utilized. The capabilities of the present numerical model are satisfactorily tested by comparing the instantaneous axial velocities with the existing data in various parameters. The time-mean axial velocity profiles are substantially unaffected by the changes in β and A. For high frequencies, the prominent effect of pulsations is felt principally in a thin layer near the solid wall. Skin friction is generally greater than that of a steady flow. The influence of oscillation on skin friction is appreciable both in terms of magnitude and phase relation. Numerical results for temperature are analyzed to reveal significant heat transfer characteristics. In the downstream fully established region, the Nusselt number either increases or decreases over the steady-flow value, depending on the frequency parameter, although the deviations from the steady values are rather small in magnitude for the parameter ranges computed. The Nusselt number trend is amplified as A increases and when the Prandtl number is low below unity. These heat transfer characteristics are qualitatively consistent with previous theoretical predictions.

Keywords: developing region; pulsating flow in a pipe; skin friction; heat transfer

Introduction

The importance of unsteady internal flows has long been recognized. Of much practical interest are the situations in which pulsations are superimposed on a mean flow inside a geometrically simple configuration, such as a pipe or a channel. Industrial applications can readily be found in ducts, manifolds, and combustor pipes, to cite a few. Pulsating flows in a pipe, and the attendant heat transfer, have also been the subject of several analytical[1,2] and experimental[3–7] investigations; they have aimed at disclosing the essential physics involved in these highly complicated, time-dependent flow processes. An early theoretical exposition was made by Uchida[1] about an oscillating flow, without consideration of heat transfer. He derived an exact solution under rather restricted conditions. Uchida[1] successfully demonstrated the relevance of the nondimensional frequency parameter β $[\equiv R(\omega/\nu)^{1/2}]$, where R is the pipe radius, ω the frequency of oscillation, and ν the kinematic viscosity of the fluid. One notable finding based on this classical theoretical model was that the phase lag of the velocity field from the pressure gradient varies from zero for steady motion and to 90° at the limit when the frequency is very large. Atabek and Chang[2] utilized an analytical approach to study pulsating flows under the assumption that the velocity in the inertia terms remains the same as it was at the entrance section of the pipe. In addition to these relatively early analytical accounts, other investigators vigorously pursued theoretical endeavors for the general problems of unsteady fluid flows. Lighthill,[8] in a physically insightful analysis of unsteady flows about a flat plate, laid the groundwork for analytical treatments of pulsating flows in various geometrical configurations.

On the experimental front, measurements of unsteady flow characteristics have been obtained by a variety of techniques, e.g., Atabek *et al.*[3] and Florio and Mueller[4] by hot-film anemometer, Denison *et al.*[5,6] by laser doppler anemometer, and Clamen and Minton[7] by the hydrogen-bubble method, to name a few. These velocity measurements agreed satisfactorily with the theoretical predictions of Uchida[1] and Atabek and Chang.[2] The available experimental data on heat transfer in pulsating flow in a pipe have been inconclusive, and they often show conflicting results. Some investigators reported heat transfer enhancements,[9–11] whereas heat transfer reductions were also noted by some workers.[12] In some instances, both heat transfer augmentation and reduction were detected in a single experiment.[13–15]

Some of these more obvious discrepancies can be traced to differences in the parameter spaces that were examined, as well as the nonuniformities in experimental methodologies utilized in various research efforts. An early work by Siegel[16] addressed the heat transfer characteristics of pulsating flows in a parallel channel. Invoking the slug-flow assumption, his analysis indicated that, for the case of constant wall temperatures, the presence of oscillations only slightly altered total heat transfer. In another recent development, Siegel[12] argued that, for forced convection in slow laminar flow in a channel with uniform heat addition, flow oscillations reduced the heat transfer coefficient.

Perusal of the literature on pulsating flows clearly reveals that the above-cited analytical work has been limited in parameter scope and solution methodologies. This shortcoming is unavoidable in light of the inherent and formidable difficulties involved in analytical treatments of such complicated physical problems. The experimental programs produced some useful velocity measurement data under restricted conditions. How-

Address reprint requests to Dr. Hyun at the Department of Mechanical Engineering, Korea Advanced Inst. Science and Technology, P.O. Box 150, Chong Ryang, Seoul, Korea.

Received 3 November 1989; accepted 4 June 1990

ever, as stated previously, definitive experimental information on heat transfer is conspicuously scanty. In summary, the previous accounts significantly contributed to our fundamental understanding of unsteady flow processes. However, in order to gain more concrete knowledge of flow details and heat transport characteristics in particular, it is natural to seek more versatile and powerful methods to deal with the problem. Such alternative methods are also vital to verifying existing analytical and/or experimental data.

One promising avenue is to obtain numerical solutions to the appropriate equations that govern flow phenomena. Because of the complexities of the flows and difficulties in coding, constructing a reliable and accurate numerical algorithm to calculate the unsteady flow equations remains a formidable undertaking. However, owing to the recent progress in numerical solution techniques and expanded computer resources, improved numerical procedures have been developed that will compute unsteady boundary layer flows in simple geometry. In a series of publications, Kwon *et al.*[17] proposed an updated numerical scheme to solve general unsteady, two-dimensional (2-D) boundary-layer flows. This procedure utilized the primitive variables and adopted an extension of the fully implicit numerical algorithm. In an effort to validate the accuracy and capabilities of their numerical model, several simple exemplary calculations were made for well-known canonical unsteady flows. The computed results for the sample flows agreed well with the available measurements and/or theoretical predictions. These positive comparisons have given credence to the numerical solution model of Kwon *et al.*[17] in calculating the unsteady boundary layer flows.

In the present work we perform comprehensive numerical computations of laminar incompressible pulsating flow in a cylindrical pipe. By confining our attention to this class of flow, the solutions obtained will be directly relevant to relatively slow-moving pulsating flows in a pipe. A prime example of these flows, among others, may be found in biofluid flows,[18] such as an idealized model of the blood stream in a blood tube and in many industrial applications. Specifically, we consider the flow at the inlet of a pipe of radius R given by

$$U_i = U_o(1 + A\cos\omega t^*) \tag{1}$$

The incoming fluid is at uniform temperature T_o, and the surface wall of the pipe is maintained at constant temperature T_w. The full, time-dependent laminar incompressible boundary-layer equation is used. The task is to describe the subsequent unsteady motions of the fluid inside the pipe and to analyze the associated heat transfer characteristics.

In summary, our intention is to carry out extensive numerical simulations by exploiting recently developed solution techniques for the time-dependent boundary-layer equations. The systematically rendered numerical results, encompassing a wide range of parameter spaces, can supply information that could be used to verify existing theoretical and experimental data. Furthermore, the numerical results can serve as useful source materials against which the outcome of future analytical and experimental investigations can be checked. More significantly, by carefully examining the numerical results, we can gain a better understanding of the salient features of flow and heat transfer characteristics. To date, such knowledge of flow details has not been made available through analytical tools and experimental observations.

Problem formulation

The time-dependent, incompressible laminar boundary-layer equations, written in axisymmetric cylindrical coordinates (x, r) with the corresponding velocity components (u, v), in non-dimensional form are

$$\frac{\partial u}{\partial x} + \frac{1}{r}\frac{\partial}{\partial r}(rv) = 0 \tag{2}$$

$$\frac{\partial u}{\partial t} + u\frac{\partial u}{\partial x} + v\frac{\partial u}{\partial r} = -\frac{\partial p}{\partial x} + \frac{1}{r}\frac{\partial}{\partial r}\left(r\frac{\partial u}{\partial r}\right) \tag{3}$$

$$\frac{\partial \theta}{\partial t} + u\frac{\partial \theta}{\partial x} + v\frac{\partial \theta}{\partial r} = \frac{1}{\mathrm{Pr}}\frac{1}{r}\frac{\partial}{\partial r}\left(r\frac{\partial \theta}{\partial r}\right) \tag{4}$$

where x denotes the axial coordinate, r is the radial distance from the pipe axis, and θ is the temperature. The thermophysical properties are ν, the kinematic viscosity, and κ, the thermal diffusivity. The appropriate nondimensional quantities have been introduced in the following manner,[19]

$$u \equiv \frac{u^*}{U_o}, \qquad v \equiv \frac{\mathrm{Re}v^*}{U_o}, \qquad p \equiv \frac{p^*}{\rho U_o^2},$$

$$\theta \equiv \frac{T - T_o}{T_w - T_o}, \qquad x \equiv \frac{x^*}{\mathrm{Re}R}, \qquad r \equiv \frac{r^*}{R},$$

$$t \equiv \frac{t^* U_o}{\mathrm{Re}R},$$

$$\mathrm{Re} \equiv \frac{U_o R}{\nu}, \qquad \mathrm{Pr} \equiv \frac{\nu}{\kappa}, \qquad \beta \equiv R\left(\frac{\omega}{\nu}\right)^{1/2}$$

in which the dimensional counterparts are indicated by an asterisk. The three principal nondimensional parameters are the mean-flow Reynolds number Re, the Prandtl number Pr, and the frequency parameter β, which appears in connection with the specification of boundary conditions. Note that in the present formulation the Reynolds number is embedded in the appropriately scaled nondimensional quantities.[19] Therefore

Notation

A	Pulsation amplitude of the inlet flow
B	Pressure gradient, $-\partial P/\partial x$
Cf	Skin friction coefficient
Nu	Nusselt number
P	Pressure
Pr	Prandtl number
R	Pipe radius
Re	Reynolds number, $U_o R/\nu$
T, θ	Dimensional, nondimensional temperature
t, t^*	Nondimensional, dimensional time
U_o	Time mean velocity at the pipe inlet
u^*, v^*	Dimensional velocity components
u, v	Nondimensional velocity components
x^*, r^*	Dimensional coordinates
x, r	Nondimensional coordinates

Greek symbols

β	Nondimensional frequency parameter
ρ	Density
ϕ	Phase angle
ν	Kinematic viscosity
ω	Pulsation frequency

within the framework of laminar boundary-layer flows, dependence of the physical variables—when expressed in nondimensional form—on Reynolds number will not be explicitly shown. When the physical quantities of interest are converted back to their dimensional values, however, the conspicuous effect of Reynolds number can be brought into focus.

At the pipe inlet, the flow is taken to be unidirectional, pulsating, and at uniform temperature:

$$\text{at } x=0, \quad u(0,r,t)=1+A\cos\beta^2 t \tag{5a}$$

$$v(0,r,t)=0 \tag{5b}$$

$$\theta(0,r,t)=0 \tag{5c}$$

The proper boundary conditions at the pipe wall surface are

$$\text{at } r=1, \quad u(x,1,t)=0 \tag{5d}$$

$$v(x,1,t)=0 \tag{5e}$$

$$\theta(x,1,t)=1 \tag{5f}$$

Owing to the symmetry requirement at the centerline, we have

$$\text{at } r=0, \quad \frac{\partial u}{\partial r}(x,0,t)=0 \tag{5g}$$

$$v(x,0,t)=0 \tag{5h}$$

$$\frac{\partial \theta}{\partial r}(x,0,t)=0 \tag{5i}$$

The governing equations are of the parabolic type. The equations are integrated by proceeding downstream; consequently, as has been amply discussed,[20] the boundary conditions at the downstream pipe exit are not prescribed.

The main task now is to find a suitable numerical solution technique for the system of partial differential equations, Equations 2–4 for the inlet and boundary conditions, Equations 5a–5i. The technique should be flexible enough to apply over a wide range of the externally specifiable parameters A and β.

Numerical method

In order to solve the system of equations described, we developed a finite-difference numerical code that is based largely on the methodologies originally proposed by Kwon *et al.*[17] We solved the differenced equations and boundary conditions by a fully implicit numerical algorithm, using the primitive variables. The specifics of the numerical solution techniques were succinctly documented by Kwon and colleagues; as stated earlier, Kwon[21] and Cho and Hyun[22] adapted these methods successfully to certain external flows.

For the internal flows under investigation, we calculated the pressure gradient following the iteration techniques of Cebeci and Bradshaw[20] together with consideration of conservation of mass. For typical computational runs, 4–6 local iterations usually were required to meet the preset convergence criteria. In the present computations, the accuracy levels between two successive iterations were 10^{-6} and 10^{-11} for the variations of streamwise velocity gradient at the wall and the pressure gradient, respectively.

For the initial state conditions, an approximate solution of steady-state flow was adopted. The temporally periodic solution was attained usually after 4–6 cycles of pulsation. To ensure sufficient temporal resolution of the numerical solution, 108 time intervals constituted one pulsating cycle. The spatial mesh used was typically (101 × 51) in the (x–r) computational domain. In a manner similar to that of Kwon *et al.*[17] and Cho and Hyun,[22] sensitivity tests to grid were conducted for several exemplary runs; the results were generally satisfactory.

Results and discussion

As is evident in the governing system of equations, Equations 2–5, a pulsating flow is characterized by the pertinent nondimensional parameters, i.e., β and A. The computational domain in the axial extent has been set $0\le x\le x_e$; for most calculations, $x_e=0.25$ was adopted. Evidently, in the case of unsteady flows, there are no definitive data indicating the axial stations where the flow becomes fully developed. However, based on the knowledge of steady flows, $x_e\simeq 0.25$ is presumed to be sufficient to encompass the entire field from the inlet to the region of fully developed flow.[19,20,23] In the present study, several test calculations were performed with varying values of x_e. The results suggest that, for all the runs computed, the spatial evolutions of the flow after $x\ge x_e\simeq 0.25$ are negligibly small; this conclusion justified the choice of $x_e=0.25$ for use in the computations. Recall that the nondimensional axial coordinate (x) is related to the dimensional quantity (x^*) by $x=x^*/\mathrm{Re}R$. The Prandtl number was set at 7.0 to model water.

In a manner similar to the previous development,[22,24,25] the time-dependent physical variables are expressed as

$$u=u_m+Au_1\cos(\beta^2 t+\phi_u) \tag{6a}$$

$$B=B_m+AB_1\cos(\beta^2 t+\phi_B) \tag{6b}$$

$$Cf=Cf_m+ACf_1\cos(\beta^2 t+\phi_c) \tag{6c}$$

$$\theta=\theta_m+A\theta_1\cos(\beta^2 t+\phi_\theta) \tag{6d}$$

$$\mathrm{Nu}=\mathrm{Nu}_m+A\mathrm{Nu}_1\cos(\beta^2 t+\phi_N) \tag{6e}$$

where Cf and Nu denote the skin friction coefficient and the Nusselt number, respectively, and B indicates the pressure gradient ($B\equiv -\partial P/\partial x$). Subscript m indicates the time-averaged part, subscript 1 represents the normalized amplitude of the pulsating part, and ϕ shows the phase advance (or lag) with respect to the velocity at the inlet.

In the actual computations, sufficiently broad ranges of externally specifiable parameters were traversed. The amplitude of pulsation contained at the inlet flow, A, was varied from a very small value to $A=0.30$. These large values of A were chosen to cover the flow situations in which nonlinearities are presumed to be significant in pulsations. Another principal parameter is the frequency parameter β. The range of β covered from the nonpulsating flow ($\beta=0$) to a high-frequency case of $\beta=15.0$. The parameter values for which experimental and analytical data exist are included within the parameter ranges of the calculations. These enable us to cross-compare results explicitly and specifically. As ascertained previously, the parameter spaces for the present study were selected so that the basic phenomena in wide ranges of externally prescribable conditions could be systematically delineated.

The velocity field

First, we present three exemplary sets of the axial velocity field u. By plotting u itself at selected time instants, we can obtain an overall view of the pulsating flows. Another advantage of the u plots is that direct comparisons with the existing experimental measurements are feasible.

Figure 1a–c illustrate the radial profiles of the axial velocity at three axial locations for $\beta=5.0$ and $A=0.344$. These particular values of β and A were chosen in order to duplicate the available analytical solutions[2] and measurements.[3] Figure 1a shows the results for an axial location in the entrance region, Figure 1b shows the results for a point slightly farther downstream, and Figure 1c is typical of the fully developed flow patterns. The present numerical results are in fair agreement with these data. As is evident in Figure 1, in the entrance region the axial velocity

profile is steep only near the wall, and the magnitudes of axial velocities are substantially uniform at small and moderate radii. In the downstream region, in which established flow exists, the average maximum velocity at the centerline reaches 2.0, and the characteristic parabolic profiles are apparent. The comparisons in Figure 1 demonstrate that the present numerical

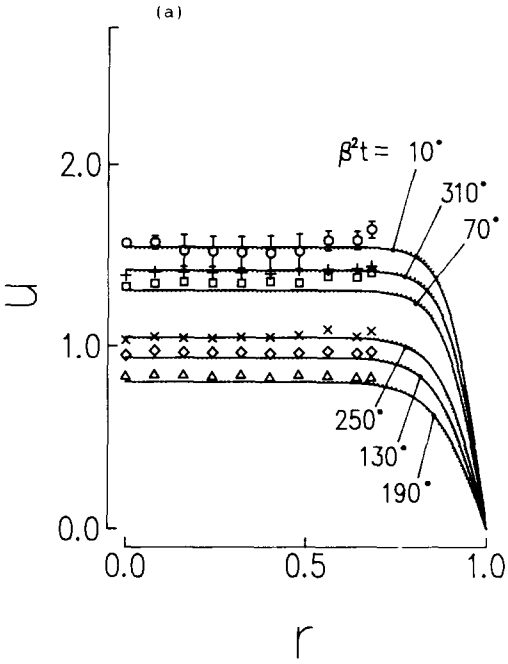

Figure 1a Instantaneous velocity profiles, u, at $x=0.005$ for $\beta=5.0$ and $A=0.344$: ——, the present calculations; · · · · ·, analytic solutions.[2] Measurements[3]: ○, 10°; □, 70°; ◇, 130°, △, 190°, ×, 250°, +, 310°

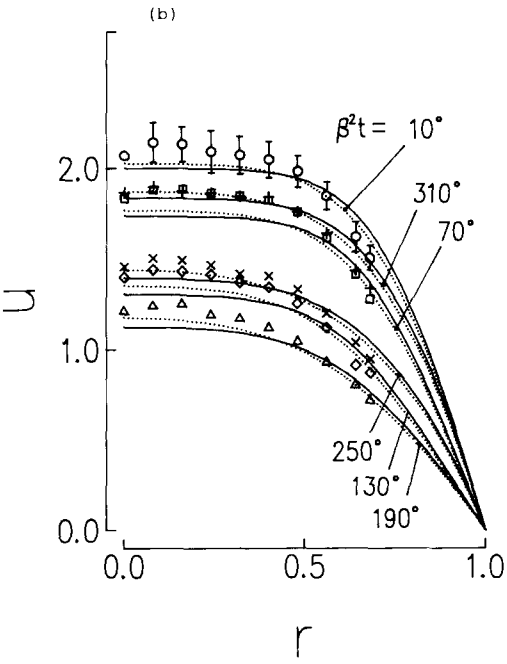

Figure 1b Instantaneous velocity profiles, u, for $\beta=5.0$ and $A=0.344$: ——, the present calculations at $x=0.0425$; · · · · ·, analytic solutions[2] at $x=0.0425$. Measurements[3] at $x=0.0432$: ○, 10°; □, 70°; ◇, 130°, △, 190°, ×, 250°, +, 310°

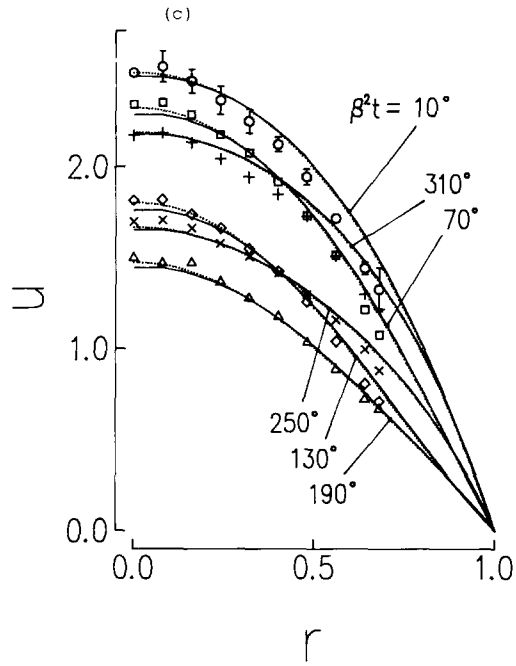

Figure 1c Instantaneous velocity profiles, u, for $\beta=5.0$ and $A=0.344$: ——, the present calculations at $x=0.25$; · · · · ·, analytic solutions[2] at $x=0.25$. Measurements[7] at $x=0.263$: ○, 10°; □, 70°; ◇, 130°, △, 190°, ×, 250°, +, 310°

calculations satisfactorily reproduce the existing velocity data throughout the entire domain of flow field and at all time instants.

Figure 2 provides further cross-comparisons—for $\beta=11.2$ and $A=0.69$—for the flow in the fully developed region. Note that this example represents a flow of high-frequency and appreciably large-amplitude pulsation. The results shown in Figure 2 clearly display overall consistency between the computations and measurements[7] for these parameter values. Another convincing example of the versatility and capability of the present numerical calculations is shown in Figure 3. These data are for a purely oscillating flow, driven by an oscillating axial pressure gradient, without a net mass throughflow. Again, the computed results agree closely with the measurements.[5] To summarize, the computed instantaneous axial velocity profiles successfully depict the characteristic time-dependent flow patterns throughout the entire flow field; these results are consistent with the other published data in a variety of parameter settings.

Exploiting the wealth of computed flow data, we now scrutinize the salient dynamic features of the pulsating flows. Our aim is to analyze the specific influence of pulsation—characterized by frequency β and amplitude A—on the global flow and heat transfer properties.

Figure 4 shows the axial variation of the pressure gradient. The amplitude is reasonably small ($A=0.1$), and a wide range of frequency parameters was adopted for calculations. The time-mean pressure gradient B_m is not altered substantially by the inlet flow oscillation parameters, i.e., A and β. The almost constant axial pressure gradient, which occurs at small distances away from the inlet, is the principal driving force maintaining the global throughflow. This phenomenon has been well documented for steady flow in a pipe. The fluctuating part of the pressure gradient, B_1, maintains nearly constant values along the pipe's length, except very close to the inlet. However, the magnitude B_1 and the phase lead ϕ_B show marked dependence on the frequency parameter β, but these factors are quite independent of amplitude A in the ranges of the present

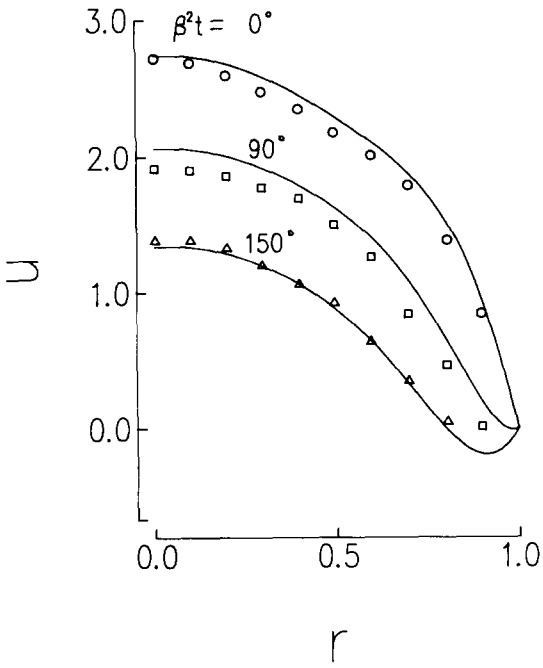

Figure 2 Instantaneous velocity profiles, u, for $\beta=11.2$ and $A=0.69$: ——, the present calculations at $x=0.25$. Measurements[7] for fully developed flow: ○, 0°; □, 90°; △, 150°

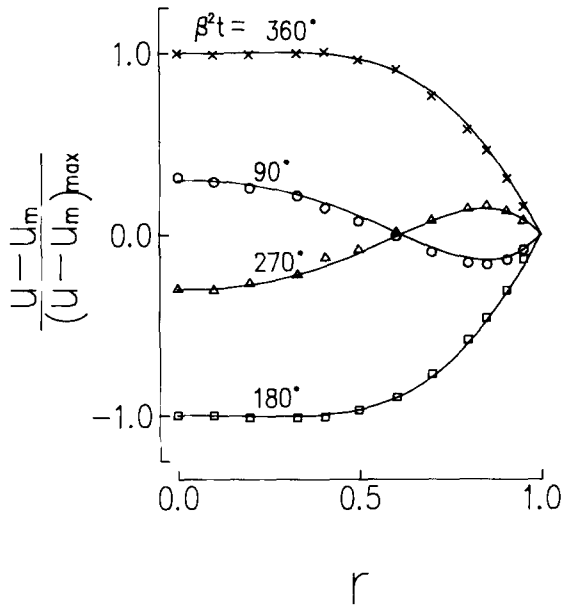

Figure 3 Normalized instantaneous velocity profiles: ——, the present calculations for $\beta=5.0$ and $A=0.344$ at $x=0.250$. Measurements[5] for $\beta=0.499$ with zero mean velocity: ○, 90°; □, 180°; △, 270°; ×, 360°

calculations. For low frequencies, B_1 is very small and ϕ_B is meager. These values imply that the impact of the pulsation is generally insignificant and that the overall deviations from the steady flow are not conspicuous. For high frequencies, the influence of pulsation is appreciable. The magnitude of the oscillating part of the pressure gradient is substantial, and the phase lead of the oscillating part of the pressure gradient over the inlet flow approaches 90°. This phase relation at high frequencies agrees with the earlier analytical treatises.[1,16]

In an effort to portray the characteristic details of flow features, we further processed the numerical data for velocities. Figure 5 depicts the spatial evolution of the time-mean velocity profiles u_m, which remained substantially unaffected by the changes in β and A. Even when $A=0.30$, the mean flow patterns

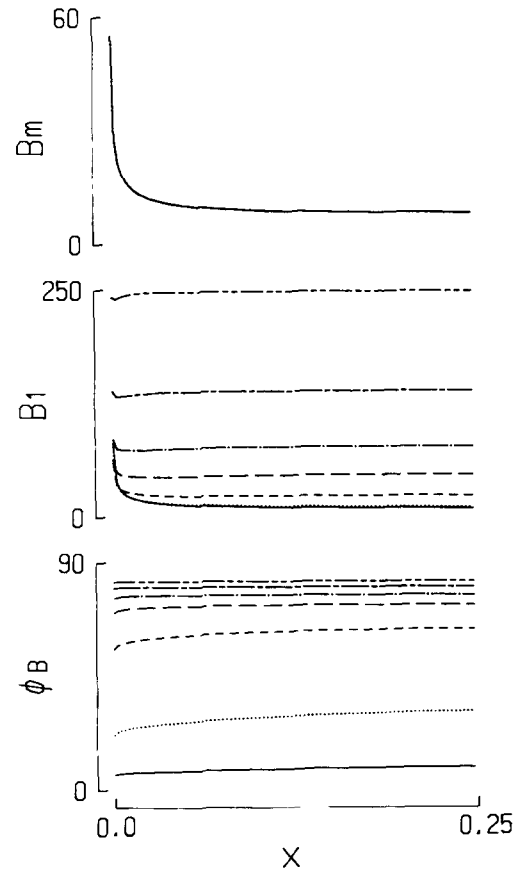

Figure 4 Plots of the pressure gradient for $A=0.1$: ——, $\beta=1.0$; · · · · ·, $\beta=2.0$; – – –, $\beta=4.0$; — — —, $\beta=6.0$; —·—·, $\beta=8.0$; ——–, $\beta=11.0$; ——–, $\beta=15.0$

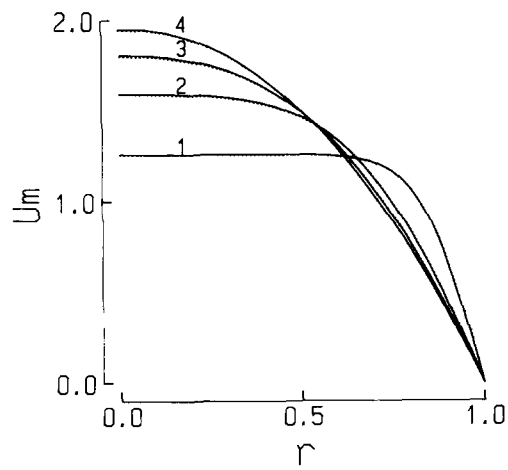

Figure 5 Profiles of the time-averaged velocity u_m. The axial locations are: 1, $x=0.01$; 2, $x=0.05$; 3, $x=0.10$; and 4, $x=0.20$. ——, steady-flow calculations; · · · · ·, calculations for $A=0.30$ and $\beta=5.0$

are not much different from those of the steady solution. Therefore the plots in Figure 5 represent the general trend of the flow patterns for the entire parameter ranges. Evolution of the u_m profiles at downstream locations is virtually the same as that for a steady flow. A similar observation was noted for pulsating flows about a flat plate. For that problem, Kwon *et al.*[17] and Cho and Hyun[22] asserted that the impact of the pulsation on the time-mean velocities was very small.

Variations of the magnitude u_1 and phase lead ϕ_u of the oscillating part of the velocity are shown in Figures 6 and 7. For low frequencies, the shape of u_1 profiles is quite similar to that of u_m, and ϕ_u itself is very small. Consequently, the influence of the oscillating part can largely be superimposed as a perturbation on the time-mean part, and the overall flows in the downstream stations are nearly in phase with the inlet flows. For high frequencies, distinctively different pictures emerge. When β is large, the shape of u_1 profiles does not vary appreciably in all axial locations. At small and moderate radii, u_1 is fairly uniform, and a sharp decline with radius is discernible close to the wall. The plots of the phase lead ϕ_u for high frequencies are also revealing; the magnitude of ϕ_u is small, and ϕ_u does not vary much with r at small and moderate radii. In a narrow region close to the wall, ϕ_u increases sharply with r, and ϕ_u reaches a value of about 40° near the wall. For high-frequency pulsations, a qualitatively similar behavior was observed for pulsating flows about a flat plate.[9,17,22] As expected for pulsations of high frequencies, the prominent effect of pulsations is felt principally in a thin layer near the solid wall.

Based on the flow data, skin friction at the pipe wall was computed. Figure 8 shows the percentage increase of the time-mean skin friction coefficient for pulsating flow Cf_m over the corresponding value of the steady flow Cf_s. In general, Cf_m is greater than Cf_s. The deviation of Cf_m from Cf_s reaches a maximum near the pipe entrance, and with increasing downstream axial distances, $(Cf_m - Cf_s)$ decreases. In the regions of fully established flow, Cf_m becomes virtually the same as Cf_s for moderate and high frequencies; this condition reflects the

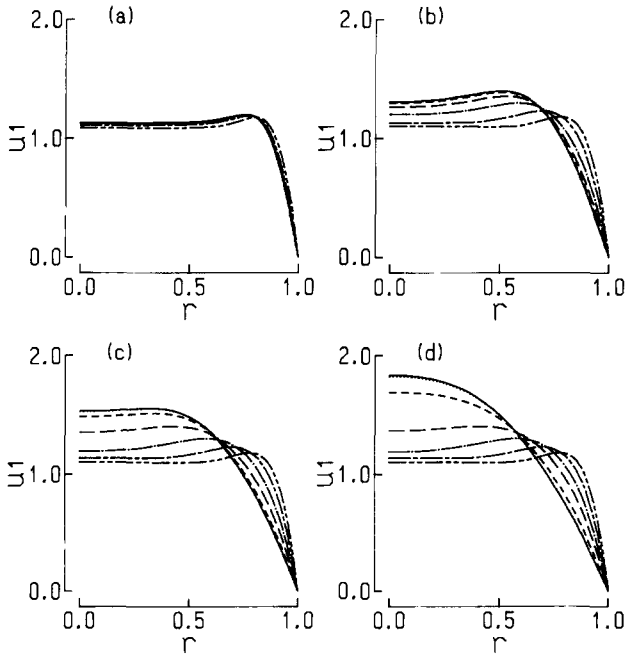

Figure 6 Amplitude of the fluctuating part of velocity, u_1, for $A=0.1$. The axial locations are: (a) $x=0.01$, (b) $x=0.05$; (c) $x=0.10$; and (d) $x=0.20$. ——, $\beta=1.0$; · · · · ·, $\beta=2.0$; – – – –; $\beta=4.0$; — — —, $\beta=6.0$; — · — · —, $\beta=8.0$; — — — —, $\beta=11.0$; — — —, $\beta=15.0$

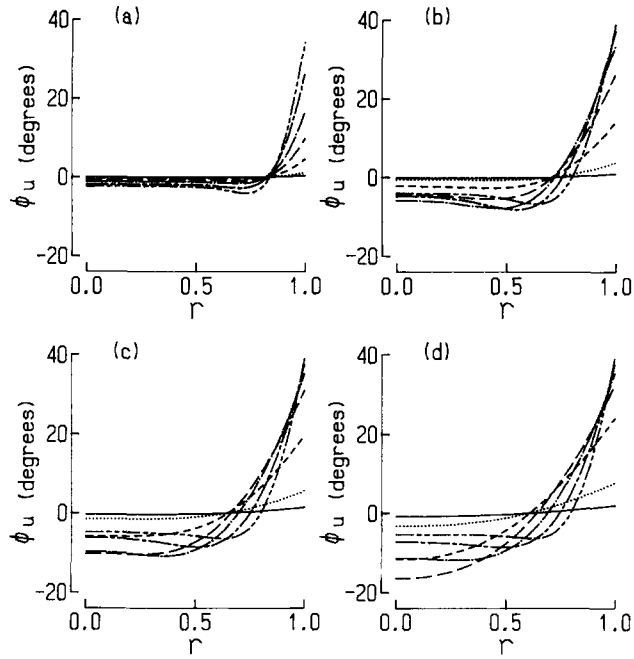

Figure 7 Phase of the fluctuating part of velocity, ϕ_u, for $A=0.1$. The axial locations are: (a) $x=0.01$; (b) $x=0.05$; (c) $x=0.10$; and (d) $x=0.20$. ——, $\beta=1.0$; · · · · ·, $\beta=2.0$; – – – –; $\beta=4.0$; — — —, $\beta=6.0$; — · — · —, $\beta=8.0$; — — — —, $\beta=11.0$; — — —, $\beta=15.0$

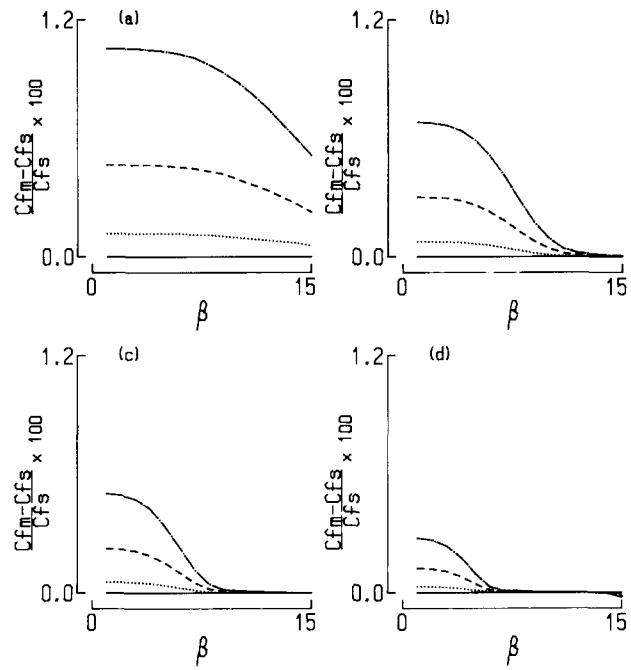

Figure 8 Plots of the time-averaged skin friction coefficient, Cf_m; Cf_s denotes the corresponding steady-flow values. The axial locations are: (a) $x=0.01$; (b) $x=0.05$; (c) $x=0.10$; and (d) $x=0.20$. ——, $A=0.01$; · · · · ·, $A=0.10$; – – –, $A=0.20$; — · — · —, $A=0.30$

negligible effect of high-frequency oscillations on the time-averaged skin friction in the fully developed flow region. As is intuitively clear, the increase of Cf_m over Cf_s becomes large as A increases. In order to more closely examine skin friction, we plotted the axial evolutions of Cf over a broad range of β in Figure 9. As stipulated earlier, the time-mean value Cf_m shows virtually no variation with β. For low frequencies, the axial

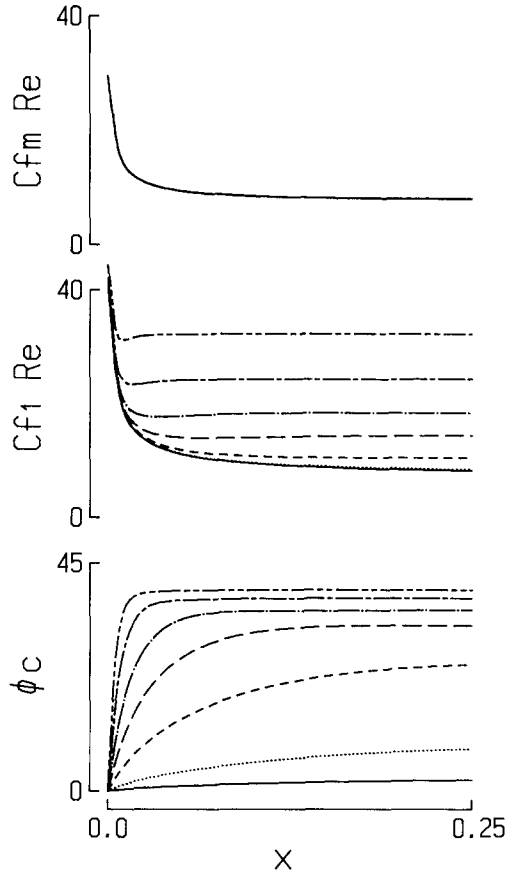

Figure 9 Axial evolutions of Cf for $A=0.1$: ——, $\beta=1.0$; · · · · ·, $\beta=2.0$; – – – –; $\beta=4.0$; — — — —, $\beta=6.0$; —·—·—, $\beta=8.0$; — — — —, $\beta=11.0$; — — — —, $\beta=15.0$

variations of Cf_1 and ϕ_c are in line with those of u_1 and ϕ_u. Hence the impact of the oscillating part of skin friction can be superposed on the overall time-mean part, and the oscillations are in phase with inlet flow conditions. For high frequencies, however, both Cf_1 and ϕ_c vary rapidly in the entrance region, and they tend to remain fairly constant with x in the bulk of flow field in the pipe. The influence of oscillation on skin friction is substantial, both in terms of magnitude and phase relation.

Note, however, that the differences between Cf_m and Cf_s, as shown in Figure 10, are merely of the order of 1 percent or less. These small differences indicate that—for the parameter values of the present computations, and in particular, for the present range of A—the effects of pulsation on overall flow characteristics are rather meager. The preceding discussion should therefore be interpreted in a qualitative sense; in practical situations, unless A is substantially greater, the global features of pulsating flow should be largely unchanged from those of steady flow.

In order to verify the reliability and accuracy of the numerical model, we compared the results of skin friction to the linearized analytical predictions of Atabek and Chang,[2] as shown in Figure 10. The two sets of results are in reasonably good agreement, both in trend and magnitude.

The temperature field

As emphasized in the introduction, one of the major objectives of investigating pulsating flow is to determine the possible alteration in heat transfer. For this purpose, analyses of the temperature field are essential. However, theoretical predictions and/or measurements of the temperature field are not readily available in the literature. Here, we obtained complete details of the temperature field, in conjunction with velocity data, by numerically integrating the governing system of equations.

Figure 11 illustrates the axial evolution of the time-averaged temperature profiles θ_m. In the entrance region, θ_m is substantially uniform up to $r\simeq 0.8$, and θ_m varies steeply in a narrow region near the wall to meet the prescribed thermal boundary condition at the wall. At locations farther downstream, the core region of constant θ_m shrinks; in the fully developed downstream positions, the constant θ_m region is confined to small radii, say, $r<0.4$. The θ_m profiles are substantially unaffected by variations in β or A; the representative plots in Figure 11 clearly show that the θ_m graphs virtually overlap the well-documented temperature profiles of the steady flow.[23]

Profiles of the oscillating part of the thermal field are shown for θ_1 in Figure 12 and for ϕ_θ in Figure 13. Note that in Equation 6d ϕ_θ denotes the phase lag of θ_1 with respect to the inlet flow

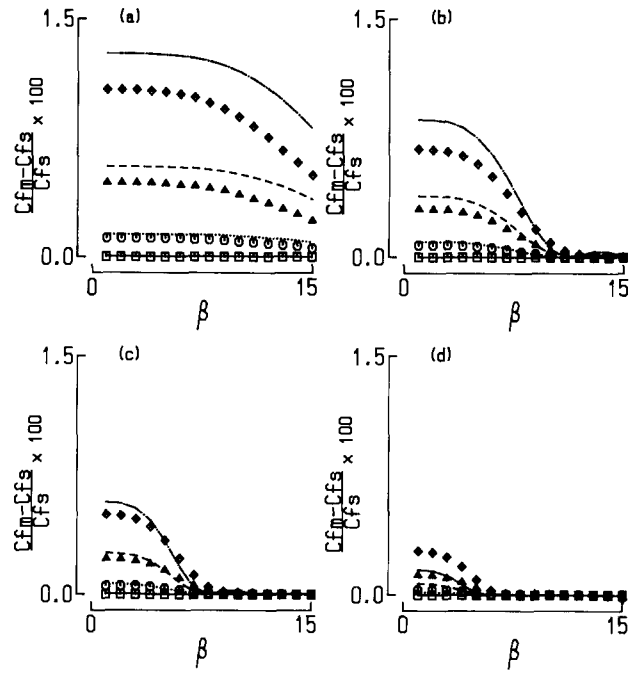

Figure 10 Comparisons of computed time-mean skin friction results, Cf_m, with analytical predictions.[2] The axial locations are: (a) $x=0.01$; (b) $x=0.05$; (c) $x=0.10$; and (d) $x=0.20$. The present calculations: □, $A=0.01$; ○, $A=0.1$; △, $A=0.2$; ◇, $A=0.3$. Analytic solutions:[2] ——, $A=0.01$; · · · · ·, $A=0.1$; – – –, $A=0.2$; —·—·—, $A=0.3$

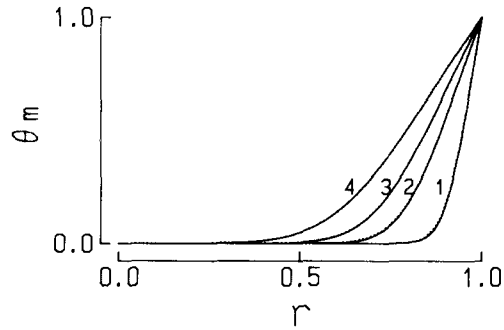

Figure 11 Profiles of time-averaged temperature θ_m. The axial locations are: 1, $x=0.01$; 2, $x=0.05$; 3, $x=0.10$; 4, $x=0.20$. ——, steady-flow calculations; · · · · ·, calculations for $A=0.30$ and $\beta=5.0$

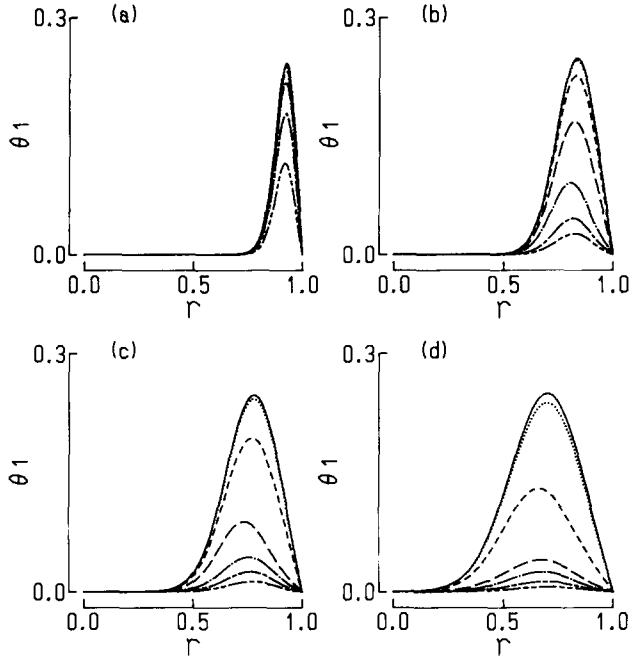

Figure 12 Amplitude of the fluctuating part of temperature, θ_1, for $A=0.1$. The axial locations are: (a) $x=0.01$; (b) $x=0.05$; (c) $x=0.10$; and (d) $x=0.20$. ——, $\beta=1.0$; · · · · ·, $\beta=2.0$; – – – –; $\beta=4.0$; — — —, $\beta=6.0$; — · — ·, $\beta=8.0$; — — — —, $\beta=11.0$; — — —, $\beta=15.0$

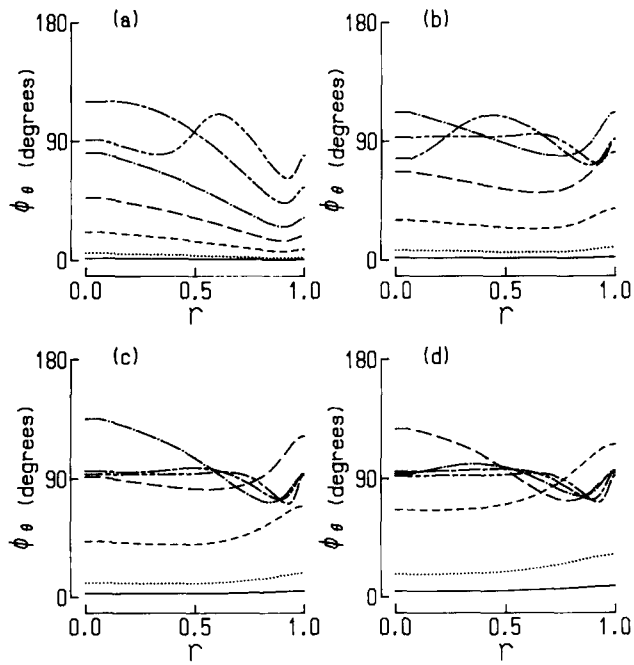

Figure 13 Phase of the fluctuating part of temperature, ϕ_θ, for $A=0.1$. The axial locations are: (a) $x=0.01$; (b) $x=0.05$; (c) $x=0.10$; and (d) $x=0.20$. ——, $\beta=1.0$; · · · · ·, $\beta=2.0$; – – – –; $\beta=4.0$; — — —, $\beta=6.0$; — · — ·, $\beta=8.0$; — — — —, $\beta=11.0$; — — —, $\beta=15.0$

conditions. Figures 12 and 13 are for a relatively small value of the prescribed amplitude of oscillation ($A=0.1$). In the entrance region, θ_1 is practically zero at small and moderate radii: θ_1 peaks at large radii before it shrinks to zero at the pipe wall. As the axial position moves in the downstream direction, the lobes of the nonzero θ_1 curves broaden. The amplitude θ_1 decreases with frequency, which contrasts to the case of the skin friction. The plots of phase lag ϕ_θ in Figure 13 disclose that at low frequencies ϕ_θ is close to zero, as can be intuitively anticipated. For high frequencies, in the downstream fully developed flow region, the oscillating part of temperature lags behind the inlet flows by 90°. Similar trends were also detected for the case of pulsating flow approaching a flat plate in the previous analytic[9] and numerical[22] works.

Figure 14 illustrates the effect of flow pulsation on the heat transfer rate, represented by the time-averaged Nusselt number Nu_m. As expected, when the amplitude of oscillation in the inlet flow is small (see the curves for $A=0.01$), the influence of pulsation is negligible; the heat transfer coefficient is about the same as that of steady flow Nu_s. In the bulk of the pipe—apart from the entrance region—Nu_m is generally lower than Nu_s for the majority of the frequency range. Only for a band of intermediate frequencies, is Nu_m greater than Nu_s. Such qualitative trends are amplified with increasing A. This observation is physically meaningful, i.e., by adding pulsation to the incoming flow at the pipe inlet, the global heat transfer rate tends to be reduced from the corresponding steady-flow value for the case of constant wall temperature. However, when the frequency parameter β falls in a narrow band of intermediate values, i.e., $\beta_1 \le \beta \le \beta_2$, where β_1 and β_2 denote the lower and upper limit of the frequency band, respectively, heat transfer is augmented by introducing pulsation. These numerical results are qualitatively consistent with theoretical predictions[26] and experimental data.[15] In particular, Barnett and Vachon[26] proposed a simplified analytical model, and they proceeded to carry out considerable mathematical manipulations. After laborious theoretical algebraic efforts, their model led to an important observation: The heat transfer rate either increases or decreases from the corresponding steady-flow value, depending on the frequency range. A specific example demonstrated that, for $Pr=0.72$ and $Re=1{,}000$, the maximum heat transfer was achieved at about $\beta=2.0$ and the enhancement of heat transfer occurred in a narrow band $0 \le \beta \le 3.3$.[26] The results

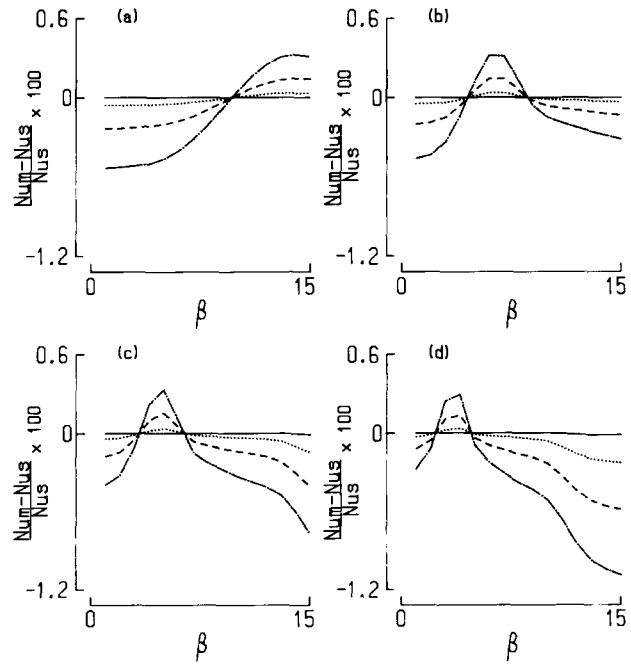

Figure 14 Plots of the time-averaged Nusselt number Nu_m; Nu_s denotes the corresponding steady-flow values. The axial locations are: (a) $x=0.01$; (b) $x=0.05$; (c) $x=0.10$; and (d) $x=0.20$. ——, $A=0.01$; · · · · ·, $A=0.10$; — — —, $A=0.20$; — · — · —, $A=0.30$

shown in Figure 14 corroborate those assertions. We gave special attention to the behavior of the Nusselt number in the fully established flow region, i.e., Figure 14d. Dependence of the Nusselt number on the frequency parameter bears strong qualitative similarity to Barnett and Vachon's analytical predictions (see Figure 2 in Reference 26).

The magnitudes of $(Nu_m - Nu_s)/Nu_s$ are important. Note that the ordinates in Figure 14 (and Figure 16) indicate that the discrepancies between Nu_m and Nu_s are on the order of 1 percent. Based on our numerical results for the parameter values, the overall impact of pulsation on the time-mean heat transfer is minor. For the values of A (≤ 0.3) adopted in the present study, the influence of pulsation on the global time-mean patterns and heat transfer seems insignificant. The analytical results presented in Reference 26 also gave the magnitudes of $(Nu_m - Nu_s)/Nu_s$ as less than 1 percent. The present results, together with those predictions, lead to an elusive point. That is, although the dependence of Nu_m on β shows a certain qualitative trend, physical interpretations should be made with care, because the magnitudes are much too small to produce a definitive statement. These assessments clearly point to a need for computing flows for much larger values of A than those used in the present calculations. The present study also underscores the potential importance of the nonlinear effects, as they are introduced by increasing A.

Figure 15 illustrates the axial evolution of heat transfer. As the axial location moves downstream, Nu_m decays rapidly from a very large value near the entrance, and the axial decrease of Nu_m becomes less steep in the bulk of the pipe soon after leaving the entrance region. These results have been well documented

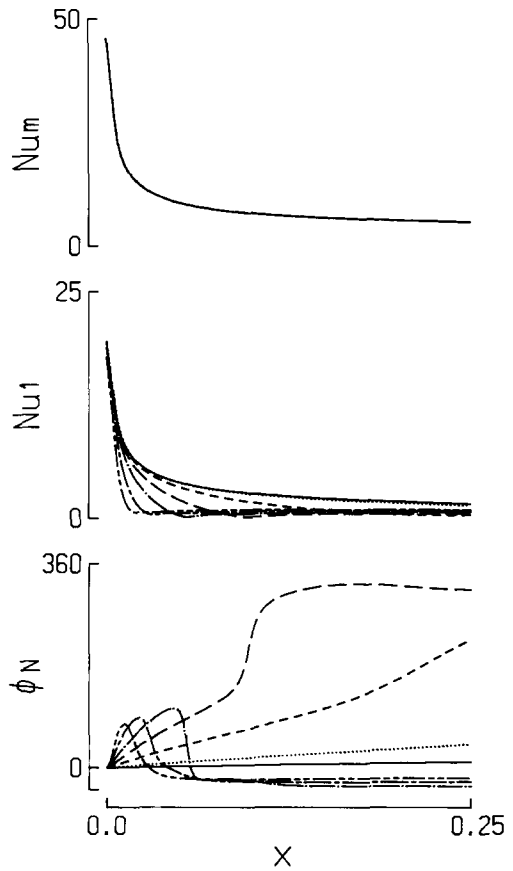

Figure 15 Axial evolutions of Nu for $A = 0.1$: ——, $\beta = 1.0$; · · · · ·, $\beta = 2.0$; – – – –; $\beta = 4.0$; — — —, $\beta = 6.0$; —·—·, $\beta = 8.0$; — — —, $\beta = 11.0$; ——–, $\beta = 15.0$

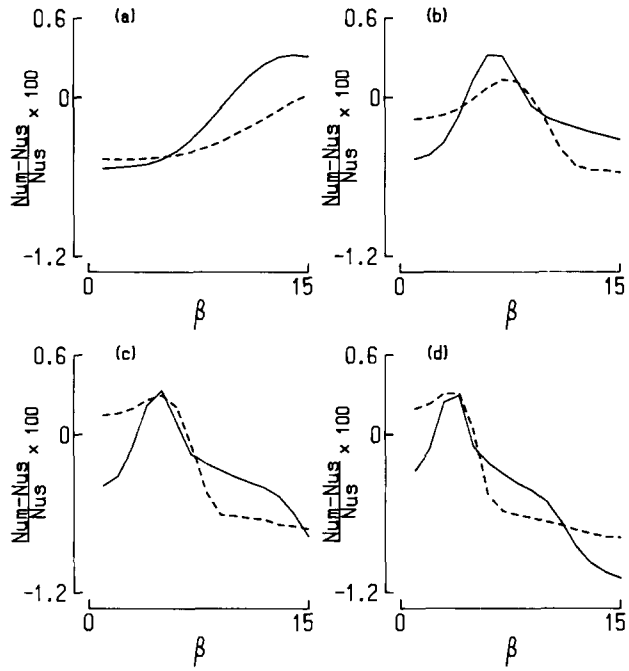

Figure 16 The effect of Pr on Nu_m; Nu_s denotes the corresponding steady-flow values; $A = 0.3$. The axial locations are: (a) $x = 0.01$; (b) $x = 0.05$; (c) $x = 0.10$; and (d) $x = 0.20$. ——, Pr = 7.0; – – – –, Pr = 0.72

for the case of steady pipe flow. For low frequencies, the shape of the Nu_1 curve is similar to that of Nu_m, and ϕ_N is practically zero throughout the entire pipe length. For high frequencies, the amplitude of the oscillating part Nu_1 decays with x much faster near the entrance region, and Nu_1 has very small values in the bulk of the flow field away from the entrance region. The behavior of ϕ_N for high frequencies is also notable. Only in the entrance region does the phase of Nu lag that of the inlet flow—by about 40°.

Another significant contention of Barnett and Vachon's theoretical model[26] was the appreciable effect of Prandtl number on the heat transfer rate. For the fully established flow field, they predicted that the alterations in heat transfer caused by pulsation would be magnified for fluids of low Prandtl numbers. However, they provided no quantitative data to verify this conclusion. We constructed Figure 16 to display the effect of Prandtl number based on the present numerical results. Figure 16d shows that, in the downstream fully developed flow region, for low and moderate values of the frequency parameter, the characteristic trend detectable in the Nu_m curves is further amplified when the Prandtl number has a small value below unity. Such qualitative consistency between the present numerical results and the previous theoretical predictions[26] is encouraging.

In summary, the elaborate numerical results for heat transfer of a pulsating flow are useful; these computed details can serve as source materials against which further experimental and analytical data may be checked for consistency. The present numerical findings suggest that the heat transfer augmentation in the established flow regions takes place only for a certain band of frequencies. For extreme low and high frequencies, heat transfer is actually reduced below that for steady flow.

Conclusions

Comprehensive and elaborate numerical data were compiled to delineate the flow and heat transfer characteristics for

pulsating flows in a pipe. The computed instantaneous axial velocity profiles were shown to be in close agreement with available measurements.

The time-averaged axial velocity distributions remain largely unaffected by the changes in β and A. For high-frequency oscillations, the effect of pulsation is felt principally in a thin layer near the solid wall. For low frequencies, the shape of u_1 profiles is similar to that of u_m, and ϕ_u is very small. In the region of fully developed flow, the time-averaged skin friction Cf_m is virtually the same as that of steady flow for moderate and high frequencies. For low frequencies, the impact of the oscillating part of skin friction can be superposed on the overall time-mean part, and the oscillations are in phase with the inlet flow conditions.

The numerical results for heat transfer rates are revealing. The time-averaged Nusselt number Nu_m either increases or decreases over the steady-flow value, depending on the frequencies. This characteristic behavior Nu_m curves versus β is more pronounced as A increases. Also significant is that, for fluids having low values of the Prandtl number below unity, the deviation of Nu_m from Nu_s, the steady-flow value, becomes more prominent. These qualitative findings support the conclusions obtained by theoretical analyses.[26]

References

1 Uchida, S. The pulsating viscous flow superposed on the steady laminar motion of incompressible fluid in a circular pipe. *ZAMP*, 1956, **7**, 403–422

2 Atabek, H. B. and Chang, C. C. Oscillatory flow near the entry of a circular tube. *ZAMP*, 1961, **12**, 185–201

3 Atabek, H. B., Chang, C. C., and Fingerson, L. M. Measurement of laminar oscillatory flow in the inlet length of a circular tube. *Phys. Med. Biol.*, 1964, **9**(2), 219–227

4 Florio, P. J. and Mueller, W. K. Development of a periodic flow in a rigid tube. *Trans. ASME J. of Basic Eng.*, 1968, 395–399

5 Denison, E. B. and Stevenson, W. H. Oscillatory flow measurements with a directionally sensitive laser velocimeter. *Rev. Sci. Instr.*, 1970, **41**(10), 1475–1478

6 Denison, E. B., Stevenson, W. H., and Fox, R. W. Pulsating laminar flow measurements with a directionally sensitive laser velocimeter. *AIChE J.*, 1971, **17**(4), 781–787

7 Clamen, M. and Minton, P. An experimental investigation of flow in an oscillating pipe. *J. Fluid Mech.*, 1977, **81**, 421–431

8 Lighthill, M. J. The response of laminar skin friction and heat transfer to fluctuations in the stream velocity. *Proc. Roy. Soc.*, 1954, **224A**, 1–23

9 Faghri, M., Javdani, K., and Faghri, A. Heat transfer with laminar pulsating flow in a pipe. *Lett. Heat Mass Transfer*, 1979, **6**, 259–270

10 Hwang, M. F. and Dybbs, A. Heat transfer in a tube with oscillatory flow. ASME paper 83-WA/HT-90, 1983, 1–12

11 Linke, W. *ZVDI*, 1953, **95**, 1179 (quoted in Reference 13)

12 Siegel, R. Influence of oscillation-induced diffusion on heat transfer in a uniformly heated channel. *Trans. ASME J. of Heat Transfer*, 1987, **109**, 224–247

13 Havemann, H. A. and Narayan Rao, N. N. Heat transfer in pulsating flow. *Nature*, 1954, **7**, 41

14 Park, J. S., Taylor, M. F., and McEligot, D. M. Convective heat transfer for ship propulsion. *7th Annual Summary Report*. University of Arizona, Tucson, AZ, 1982

15 Mamayev, V. V., Nosov, V. S., and Syromyatnikov, N. I. Investigation of heat transfer in pulsed flow of air in pipes. *Heat Transfer—Soviet Research*, 1976, **8**(3), 111–116

16 Siegel, R. and Perlmutter, M. Heat transfer for pulsating laminar duct flow. *Trans. ASME J. of Heat Transfer*, 1962, 111–123

17 Kwon, O. K., Pletcher, R. H., and Delaney, R. A. Solution procedure for unsteady two-dimensional boundary layers. *ASME Journal of Fluids Eng.*, 1988, **110**, 69–75

18 Pedley, T. J. *The Fluid Mechanics of Large Blood Vessels*, Cambridge University Press, 1980

19 Ward-Smith, A. J. *Internal Fluid Flow; The Fluid Dynamics of Flow in Pipes and Ducts*, Clarendon Press, Oxford, 1980

20 Cebeci, T. and Bradshaw, P. *Momentum Transfer in Boundary Layers*, McGraw-Hill, New York, 1977

21 Kwon, O. K. Calculation of unsteady turbulent boundary layers. ASME paper 87-GT-53, 1987, 1–8.

22 Cho, H. W. and Hyun, J. M. Motion and heat transfer in the blasius flow containing a pulsating component. *Int. J. Heat and Fluid Flow*. 1989, **10**(4), 349–356

23 Schlichting, H. *Boundary-Layer Theory*, 7th ed., McGraw-Hill, New York, 1979

24 Ackerberg, R. C. and Phillips, J. H. The unsteady laminar boundary layer on a semi-infinite flat plate due to small fluctuations in the magnitude of the free-stream velocity. *J. Fluid Mech.*, 1972, **51**, 137–157

25 Cebeci, T. Calculation of unsteady two-dimensional laminar and turbulent boundary layers with fluctuations in external velocity. *Proc. Roy. Soc.*, 1977, **355A**, 225–238

26 Barnett, D. O. and Vachon, R. I. An analysis of convective heat transfer for pulsating flow in a tube. *Proc. 4th Int. Heat Transfer Conference*, Paris, 1970, 1–11